

ProSAS: An O-RAN Approach to Spectrum Sharing between NR and LTE

Sneihil Gopal^{‡†}, David Griffith^{*}, Richard A. Rouil^{*} and Chunmei Liu^{*}

[‡]PREP Associate, National Institute of Standards and Technology (NIST), USA

[†]Department of Physics, Georgetown University, USA

^{*}National Institute of Standards and Technology (NIST), USA

Emails: {sneihil.gopal, david.griffith, richard.rouil, chunmei.liu}@nist.gov

ABSTRACT

The Open Radio Access Network (O-RAN), an industry-driven initiative, utilizes intelligent Radio Access Network (RAN) controllers and open interfaces to facilitate efficient spectrum sharing between LTE and NR RANs. In this paper, we introduce the Proactive Spectrum Adaptation Scheme (ProSAS), a data-driven, O-RAN-compatible spectrum sharing solution. ProSAS is an intelligent radio resource demand prediction and management scheme for intent-driven spectrum management that minimizes surplus or deficit experienced by both RANs. We illustrate the effectiveness of this solution using real-world LTE resource usage data and synthetically generated NR data. Lastly, we discuss a high-level O-RAN-compatible architecture of the proposed solution.

I. INTRODUCTION

The surge in multimedia applications and the rapid digitization of many industries have led to increased mobile data usage in recent years [1]. To address this growing need for data connectivity, the 3rd Generation Partnership Project (3GPP) is deploying the fifth generation (5G) radio interface known as New Radio (NR) [2]. NR is expected to meet the rising demand for data traffic and enhance wireless connectivity for various emerging applications such as automotive, healthcare, public safety, and smart cities. It is engineered to deliver high data rates, low latency, and extensive coverage and will operate within two frequency bands: Frequency Range 1 (FR1), from 410 MHz to 7.125 GHz (also known as the sub-6 GHz band), and Frequency Range 2 (FR2), from 24.25 GHz to 52.6 GHz (also called the mmWave band). As most low-frequency bands are already allocated to 4G Long Term Evolution (LTE) networks, network operators face the challenge of either acquiring new spectrum or repurposing existing LTE spectrum for NR. Both options entail substantial costs. Moreover, since LTE will continue to handle most data traffic in the near term, reallocating low-frequency bands from LTE to NR without a concurrent expansion of NR-capable devices will congest LTE bands and degrade network performance. Hence, operators need to strategically utilize their existing 4G infrastructure during the transition to NR while providing services for legacy devices. This is necessary as LTE and NR networks are expected to coexist for the foreseeable future.

To ensure a smooth transition from LTE to NR networks while supporting legacy devices and maintaining network performance, 3GPP has proposed a comprehensive set of solutions [3]. These include LTE-compatible NR numerology with a 15 kHz subcarrier spacing for unified time/frequency resource grids. Also, solutions include resource reservation, and downlink (DL) subcarrier puncturing to support enhanced Machine-Type Communication (eMTC) (Technical Report (TR) 37.823), and mechanisms for resource allocation within NR carriers for Narrowband-Internet of Things (NB-IoT) (TR 37.824). Lastly, to help mitigate and manage interference for applications like V2X (TR 37.985), 3GPP has introduced guard bands, dynamic and static power sharing mechanisms, and requirement-based access technology prioritization.

While these solutions lay a strong foundation for LTE and NR network coexistence, real-world scenarios, diverse network environments, regulations, and evolving technological demands necessitate additional adaptations. The Open Radio Access Network (O-RAN) initiative, with its open interfaces, virtualization, and intelligence, supports innovation within networks. Equipped with Artificial Intelligence/Machine Learning (AI/ML)-capable RAN Intelligent Controller (RIC), O-RAN enables advanced spectrum sharing. Within this framework, we propose Proactive Spectrum Adaptation Scheme (ProSAS), a data-driven, O-RAN-compatible resource-sharing solution. ProSAS capitalizes on O-RAN's capabilities, focusing on intelligent demand prediction and resource allocation to minimize resource surpluses or deficits experienced by networks.

We utilize statistical models and deep learning techniques to analyze and predict radio resource demand patterns. This analysis uses real-world LTE resource usage data collected using BladeRF Software Defined Radio (SDR)¹ and Online Watcher of LTE (OWL), an open-source LTE sniffer [4], as well as NR data generated synthetically using Time-Series Generative Adversarial Network (TimeGAN) [5]. The proposed scheme is O-RAN-compatible and can be implemented within the O-RAN architecture as follows: the modeling and

¹Certain commercial equipment, instruments, or materials are identified in this paper in order to specify the experimental procedure adequately. Such identification is not intended to imply recommendation or endorsement by National Institute of Standards and Technology (NIST), nor is it intended to imply that the materials or equipment identified are necessarily the best available for the purpose.

training processes corresponding to demand prediction can occur within the non-real-time (non-RT) RIC, leveraging data gathered from Radio Access Network (RAN). The optimal model can be selected and subsequently deployed to the near-real-time (near-RT) RIC for inference. During the inference phase, the near-RT RIC can allocate resource blocks to minimize any surplus or deficit for both RANs. To demonstrate ProSAS’s compatibility with O-RAN requirements, we discuss a high-level architectural overview of the modules and the deployment scenario alongwith a summary of the end-to-end workflow involved. To the best of our knowledge, this paper is the first attempt to propose an O-RAN-compatible scheme that manages radio resources proactively and intelligently to balance the demands of LTE and NR networks. Our use of real-world data and alignment with industry standards makes this proposal practical and pertinent for network operators. Furthermore, we provide a valuable set of LTE resource usage data for researchers, and we demonstrate the utility of a GAN in generating synthetic radio resource usage data [6].

The structure of the paper is as follows: Section II delves into related work. Section III provides an overview of O-RAN, the ProSAS framework, and the high-level architecture of the O-RAN-compatible deployment scenario. The effectiveness of ProSAS is demonstrated in Section IV. Finally, Section V concludes the paper.

II. RELATED WORK

In addition to 3GPP’s work, the research community has also studied LTE-NR coexistence [7]–[13]. In [7], the authors addressed co-channel interference, and proposed a low-complexity interference mitigation method for NR devices. In [8], the authors presented experimental results for LTE-NR coexistence in the 700 MHz band, demonstrating peaceful DL coexistence. In [9], the authors introduced a spectrum exploitation mechanism balancing transmission efficiency, coverage, and latency. In [10], the authors discussed LTE-NR uplink (UL) coexistence, revealing that LTE needs a single resource block as a guard band, while NR remains unaffected by LTE. In [11], the authors explored LTE Frequency Domain Duplex (FDD) and NR FDD coexistence in the 2.1 GHz band and showed that LTE FDD DL causes harmful interference to NR FDD DL. Conversely, [12] analyzed NR FDD and LTE Time Domain Duplex (TDD) coexistence in the 1.8 GHz band, showing their compatibility in adjacent bands. [13] explored NR UL/DL coexistence with LTE UL/DL, highlighting the role of UL sharing in balancing spectrum efficiency, latency, coverage, and channel bandwidth. Additionally, LTE-NR coexistence has been examined for specific applications like eMTC [14], NB-IoT [15], and V2X [16].

While the existing work on LTE-NR coexistence has made significant strides, several aspects can be improved with the integration of O-RAN principles. One missing element is adaptability and intelligent management of resources to proactively balance the demands of LTE and NR networks, which is our focus. We will show how this element can support spectrum sharing, which has recently gained the attention of

the O-RAN Alliance Working Group 1 (WG1) [17] and has been explored in several studies [18]–[21]. In [18], the authors propose spectrum sharing between government Low Earth Orbit satellites and 5G UL using O-RAN intelligence and open interfaces. In [19], a Reinforcement Learning (RL)-based radio resource management solution is developed, leveraging the O-RAN platform. [20] introduced O-RAN-compliant frameworks for enabling spectrum sharing. Specifically, [20] demonstrated the framework’s performance in LTE-WiFi coexistence in unlicensed bands, using srsRAN for prototype development and the Colosseum channel emulator for data collection. [21] explored contextual user density data for spectrum management in O-RAN-based networks, offering numerical validation of the proposed concept. While these works make valuable contributions, ProSAS features a data-driven, intelligent, and intent-driven approach to spectrum sharing and resource management. Its use of real-world data and compatibility with O-RAN makes it a potential tool for supporting LTE-NR coexistence.

III. THE PROSAS FRAMEWORK

O-RAN represents a transformative approach to modernizing the traditional RAN. Unlike traditional RANs, which often rely on proprietary, monolithic hardware and software solutions, O-RAN promotes open interfaces and virtualization technologies and introduces near-RT RICs and non-RT RICs to coordinate and manage network resources. These RICs play pivotal roles in the O-RAN architecture by optimizing radio resource allocation, enhancing network performance, and ensuring quality of service (QoS). Furthermore, O-RAN promotes innovation by facilitating the development of RAN applications (rApps) and external applications (xApps) that can seamlessly interface with the RICs and the RAN infrastructure, providing advanced functionalities, intelligence, and adaptability. We have designed ProSAS such that it can use rApps, xApps, and open interfaces, and therefore harness the capabilities of the O-RAN architecture.

In this paper, we propose an intelligent radio resource demand prediction and management scheme for intent-driven (priority-based) spectrum management. We employ a high-level model for LTE and NR that makes few assumptions about the underlying technology. We assume that NR employs an LTE-compatible numerology with 15 kHz subcarrier spacing, resulting in identical time/frequency resource grids for both networks and we assume that both networks use a shared pool of time-frequency resources, referred to as Physical Resource Blocks (PRBs). Note that we define resource demand as the number of PRBs required by a network for data transmission. Our approach learns the resource usage patterns of each network by analyzing their individual resource usage time-series datasets, using a variety of statistical models and deep learning architectures to predict future demand. We choose the method with the lowest root-mean-square error (RMSE) as the most suitable predictor. Based on the predicted demand from the selected prediction model, we allocate resources to minimize any surplus or deficit experienced by both networks,

where a surplus indicates resource over-provisioning and a deficit represents under-provisioning, leading to packet loss or buffering. Next, we discuss the proposed framework and its high-level integration into the O-RAN architecture.

1) *Radio Resource Demand Prediction*: Understanding radio resource usage patterns is crucial for effective resource management because network operators can then mitigate the costs of unexpected spikes in data traffic. We use a toolkit of time-series predictive models that incorporates statistical methods and deep learning architectures. It includes the Autoregressive Integrated Moving Average (ARIMA) [22] model, which combines autoregressive (AR) and moving average (MA) components with differencing to handle linear dependencies in the time series data. We also use the toolkit's Exponential Smoothing (ETS) model [22] to capture data patterns, including trends and seasonality.

In addition to statistical models, our toolkit includes three deep learning models tailored for time series forecasting. The Multilayer Perceptron (MLP) Model [23] is a neural network with interconnected layers of neurons, well-suited for uncovering intricate data patterns in sequential data. The Convolutional Neural Network (CNN) Model [23], originally designed for image data, can also be applied to time series data, using convolutional layers to learn relevant features, and is useful for tasks emphasizing local patterns. Lastly, the Long Short-Term Memory (LSTM) Model [23], a category of Recurrent Neural Network (RNN), engineered to capture long-term dependencies in sequential data. Its ability to retain information over extended time intervals makes it effective for time series forecasting tasks. Our toolkit also encompasses variations of the LSTM model [23], namely, CNN-LSTM (combining the convolutional layers of CNN with the sequential modeling capability of LSTM), and Convolutional LSTM (ConvLSTM) (integrating convolutional operations within LSTM units).

To establish a performance baseline for these models, we incorporate simpler models, including the Persistence or Naive model, Moving Average (MA) model, and Moving Median (MM) model. The Persistence model sets the forecast for the next time step as the previous time step, providing a benchmark for more complex models. The MA model calculates the forecast as the average of the previous n observations, which captures short-term trends or fluctuations. Similarly, the MM model calculates the forecast as the median of the previous n observations, offering robustness against outliers and generating a smoother forecast. This set of models equips us to tackle diverse aspects of radio resource usage pattern analysis, capturing simple trends and complex dependencies in time series data.

While several metrics, such as computational time and Mean Absolute Error (MAE), are used to assess prediction model performance, we rely on the widely adopted RMSE metric [23]. RMSE quantifies the standard deviation of prediction errors and is defined as: $\text{RMSE} = \left[\frac{1}{n} \sum_{i=1}^n (f_i - \hat{f}_i)^2 \right]^{1/2}$, where n is the number of time steps in a data set and f_i and \hat{f}_i are respectively the observed and predicted resource usage at the i th time step.

2) *Optimal Resource Allocation*: We now describe how resources from a shared pool of PRBs are distributed between coexisting LTE and NR networks. We assume that the controller allocates PRBs to meet each network's resource demands at regular intervals. These intervals can represent time slots in an LTE system, 1 ms subframes, periods of several seconds, minutes, or hours, depending on the scenario.

Let N_R represent the size of the PRBs resource pool used by the controller to distribute resources (N_A for LTE and N_B for NR). The primary goal is to minimize resource surplus or deficit for both networks. Our scheme determines the optimal allocation by evaluating a performance metric that addresses the networks' varying demands. Although the scheme can support static allocation (performed once during network setup) or dynamic allocation (repeated at granularities as small as 1 ms), we focus on quasi-static resource allocation. Since resource allocation follows demand prediction, we assume that the controller has knowledge of the networks' future resource demands for a defined period (e.g., the next hour or minute) and allocates resources accordingly.

Next, we define the optimization problem (OPT) as follows:

$$\begin{aligned} \text{OPT: } & \min_{N_A, N_B} J(N_A, N_B | \gamma, x_{D_A}, x_{D_B}), \\ \text{s.t. } & N_A + N_B \leq N_R, \\ & 0 \leq N_A \leq N_R, \\ & 0 \leq N_B \leq N_R, \end{aligned} \quad (1)$$

where,

$$J = \gamma \left(\frac{N_A - x_{D_A}}{x_{D_A}} \right)^2 + (1 - \gamma) \left(\frac{N_B - x_{D_B}}{x_{D_B}} \right)^2, \quad (2)$$

is the weighted sum of squared fractional surpluses/deficits, i.e., $(N_A - x_A)/x_A$ and $(N_B - x_B)/x_B$, experienced by LTE and NR, respectively. (N_A, N_B) is the ordered pair of allocation and (x_{D_A}, x_{D_B}) is the ordered pair containing statistics associated with the distributions of LTE's and NR's respective demands, i.e., $(D_{A,i}, D_{B,i})$, for $i \in [1, n]$, where i is the time in a length- n period. $\gamma \in (0, 1)$ is the weighting factor that enables intent-driven spectrum management by allowing the controller to prioritize one network over the other. Specifically, $\gamma \rightarrow 1$ assigns a higher priority to LTE, whereas, $\gamma \rightarrow 0$ assigns a higher priority to NR.

We consider two variations of OPT: (a) OPT_{\max} which uses the maximum network demand (M_{D_A}, M_{D_B}) , as the network statistics (x_{D_A}, x_{D_B}) in Eq. (2), further substituted in Eq. (1), and (b) OPT_{avg} which uses the mean of the objective function, i.e., $E[J]$, and therefore considers the mean and variance of each network's demand.

For OPT_{avg} , the objective function is:

$$\begin{aligned} J_{\text{avg}} &= E \left[\gamma \left(\frac{N_A - D_A}{D_A} \right)^2 + (1 - \gamma) \left(\frac{N_B - D_B}{D_B} \right)^2 \right], \\ &= 1 + \gamma N_A C_A + (1 - \gamma) N_B C_B, \end{aligned} \quad (3)$$

where, by linearity of the expectation $E[\cdot]$, for $X \in \{A, B\}$,

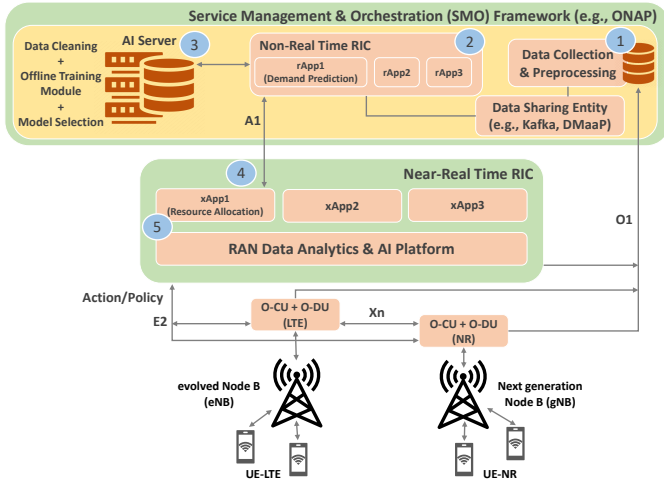


Fig. 1: High-level structure illustrating the deployment of ProSAS within the O-RAN architecture [17].

$$C_X = N_X \left(\frac{1}{\mu_{D_X}^2} + \frac{3\sigma_{D_X}^2}{\mu_{D_X}^4} \right) - 2 \left(\frac{1}{\mu_{D_X}} + \frac{\sigma_{D_X}^2}{\mu_{D_X}^3} \right), \quad (4)$$

μ_{D_A} and μ_{D_B} are the mean, and $\sigma_{D_A}^2$ and $\sigma_{D_B}^2$ are the variance of LTE and NR's demand, respectively. As with OPT_{\max} , OPT_{avg} can be obtained by substituting Eq. (3) in Eq. (1). OPT_{\max} and OPT_{avg} are both convex-optimization problems and each has a global minimum.

For the optimal resource pool partition (N_A^*, N_B^*) , we compute the average normalized surplus or deficit, denoted by S_A and S_B for LTE and NR, respectively:

$$S_A = \frac{1}{n} \sum_{i=1}^n \left(\frac{N_A^* - D_{A,i}}{D_{A,i}} \right), \quad S_B = \frac{1}{n} \sum_{i=1}^n \left(\frac{N_B^* - D_{B,i}}{D_{B,i}} \right). \quad (5)$$

Lastly, we compute the fairness of the allocations for OPT_{\max} and OPT_{avg} using Jain's Fairness Index defined as:

$$F = \frac{(N_A^* + N_B^*)^2}{2((N_A^*)^2 + (N_B^*)^2)}. \quad (6)$$

3) *Deployment Architecture*: Next, we describe how ProSAS could be implemented in the O-RAN architecture, with the structure and end-to-end flow illustrated in Fig. 1. The design and deployment scenarios are based on the guidelines outlined in the TR [24] by the O-RAN Alliance.

- ① Data collected from the RAN components (O-CU and O-DU), including the Downlink Control Information (DCI), is transmitted to the data collector in the Service and Management Orchestration (SMO) entity through the O1 interface. This data is input for the Demand Prediction rApp within the non-RT RIC.
- ② Using a data-sharing entity such as DMaP or Kafka, the gathered data is routed to the non-RT RIC in the SMO.
- ③ The relevant AI/ML models, including statistical models and deep learning architectures, in the AI server (e.g., AcumosAI) in the SMO, are queried by the non-RT RIC.



Fig. 2: Average PRB usage vs. time for LTE, NR and LTE+NR, i.e., aggregate, corresponding to time granularity of 1-hour and 1-minute.

Once these models have been trained on the AI server, the non-RT RIC is notified of the inference.

- ④ The results of the inference and associated policies are forwarded to the Resource Allocation xApp in the near-RT RIC via the A1 interface.
- ⑤ The Resource Allocation xApp configures the resource allocation solution, which is derived by solving OPT_{\max} and OPT_{avg} , and selected based on Jain's fairness index. This solution is conveyed to the RAN components using the E2 interface.

IV. NUMERICAL RESULTS FOR PROSAS

For our study, we compiled an extensive dataset of LTE scheduling information, collected at the NIST Gaithersburg campus between January and February 2023 [6]. This dataset is from downlink traffic at 2115 MHz (Band 4) and was collected using OWL [4], an online decoder of the LTE control channel. We employed a BladeRF SDR board to transmit the collected real-world LTE signals to a laptop running Ubuntu 20.04 and executing OWL to decode the signals. OWL captured the LTE DCI broadcast by the base station at the 1 ms subframe level. The dataset includes information such as the system frame number (SFN), subframe index, radio network temporary identifiers (RNTIs), the number of PRBs allocated to devices, modulation and coding scheme (MCS), and DCI message type. We extracted the number of PRBs corresponding to data transmissions, specifically DCI format 2B. We also included timestamps reflecting when this data was collected, resulting in a time series dataset detailing PRB allocations for the LTE network. Importantly, this data contains no user-specific information, ensuring complete anonymity.

Due to the lack of availability of tools that can capture NR resource usage data, using the compiled real-world LTE dataset, we generated a synthetic PRB allocation dataset corresponding to the NR network. To create this synthetic NR dataset, we leveraged TimeGAN [5], a tool that generates synthetic time-series data by capturing temporal dependencies through RNN. We used TimeGAN and the collected real-world LTE time-series data to produce synthetic time-series NR

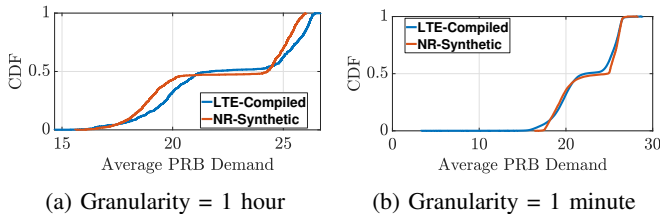


Fig. 3: CDF of average PRB demand for LTE and synthetically generated NR dataset for time granularity 1-hour and 1-minute.

data that closely mirrors the statistical properties and patterns observed in the LTE data. This approach is valid due to our assumption that NR employs an LTE-compatible numerology with 15 KHz subcarrier spacing, and shares an identical time-frequency resource grid. We also assumed that NR systems would serve LTE devices.

For our analysis, we performed a resampling of the time-series data, transitioning from PRB allocation per millisecond to PRB allocation per hour and per minute by using the mean function. Consequently, we obtained datasets representing the average PRB allocation for both LTE and NR per hour and minute. The former dataset comprises approximately 860 samples, while the latter encompasses approximately 49 554 samples. We defer the analysis for time granularities less than 1 minute for future research. Fig. 2 displays the average PRB usage/demand over time for LTE, NR, and the combined (LTE+NR) datasets, both at 1-hour and 1-minute granularities. Additionally, Fig. 3 shows the cumulative distribution function (CDF) of PRB demands from both networks at different granularities. This graph highlights the similarity in demand distribution between the compiled LTE dataset and the synthetically generated NR dataset, thereby confirming the effectiveness of TimeGAN. Next, we delve into the outcomes of the various resource demand prediction models, in addition to those pertaining to the resource allocation schemes.

As mentioned earlier, our comprehensive demand prediction toolkit comprises various models, combining both statistical approaches and deep learning architectures. We perform a comparative analysis, evaluating the performance of these models against alternatives like the Persistence or Naive model, MA model, and MM model. The implementation of these prediction models is carried out in Python, with Keras serving as the backend for deep learning architectures. For each model, we have designed a framework for grid-searching model hyperparameters, employing RMSE as our guiding metric through one-step walk-forward validation. The selected hyperparameters for each model are listed in Table I for transparency and reproducibility. For training and validating the model architecture, we use 66 % for training at each granularity, i.e., 1-hour and 1-minute [22]. Lastly, for the deep learning architectures, we use the Adam optimization algorithm [22] and employ Rectified Linear Unit (ReLU) as the activation function. In Fig. 4, we compare the prediction models based on RMSE for both networks and granularities. Notably, ARIMA outperforms other models for LTE data, whereas the ConvLSTM model has the lowest RMSE for NR data. This highlights the need for tailored models rather than a

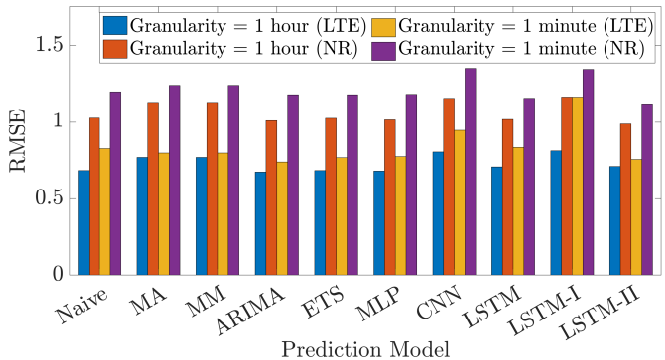


Fig. 4: Evaluation of prediction models in terms of RMSE. LSTM-I and LSTM-II refer to CNN-LSTM and ConvLSTM, respectively.

one-size-fits-all approach. Also, our results indicate that while complex deep-learning architectures can be effective, simpler statistical models can also yield strong performance.

Next, we assess the effectiveness of our resource allocation scheme. We conducted a comprehensive analysis encompassing three distinct resource pool sizes, $N_r \in \{10, 40, 50\}$ corresponding to limited, moderate, and adequate resource availability. We varied the parameter γ within each pool size configuration between 0 and 1. For each value of γ , we leveraged statistical insights derived from the predicted demand profiles of LTE and NR to determine the optimal partition sizes, N_A^* and N_B^* , under two distinct allocation strategies: OPT_{avg} (utilizing demand statistics like means and variances) and OPT_{max} (relying on demand maxima). Our evaluation aimed to capture the average surplus or deficit (see Eq. (5)) under each scenario, as well as Jain’s fairness index (see Eq. (6)), for different γ values and across various resource pool sizes (N_r). In the interest of brevity, we present results corresponding to the predicted data for LTE and NR obtained through ARIMA and ConvLSTM, respectively, at a granularity of 1 hour when $N_r = 10$ resources, as depicted in Fig. 5. It is important to note that our insights hold consistently across different granularities. Key statistics characterizing the demand profiles of LTE and NR include the following metrics: the mean demand, $\mu_{D_A} = 21.52$ and $\mu_{D_B} = 22.80$; the variances, $\sigma_{D_A}^2 = 12.37$ and $\sigma_{D_B}^2 = 8.33$; and the maxima, $M_{D_A} = 26.31$ and $M_{D_B} = 25.80$. Consequently, the expected total demand approximates 45 resources per hour, while the maximum total demand approaches 53 resources per hour.

In scenarios with $N_r = 10$ resources, where resources are scarce and lag behind demand, both networks face starvation. Total starvation, which occurs when the networks receive no resources, corresponds to a fractional deficit of -1 . Our findings (Fig. 5b) indicate that OPT_{avg} mitigates starvation over a wider range of γ values compared to OPT_{max} . Furthermore, OPT_{avg} achieves fairer allocation across a broader spectrum of γ values (Fig. 5c). For $N_r = 40$ resources, with a moderate pool size that can accommodate mean and maximum demands but falls short of the aggregate demand, OPT_{avg} achieves a perfectly fair allocation ($F = 1$) within a specific range of γ values ($\gamma \in [0.76, 0.87]$), surpassing the fairness achieved by OPT_{max} ($\gamma \in [0.47, 0.49]$). However, OPT_{avg} may result

Model	Training Hyperparameters	LTE (1-hour)	NR (1-hour)	LTE (1-minute)	NR (1-minute)
Naive	(length of historical data, offset)	(1, 1)	(1, 1)	(1, 1)	(1, 1)
MA	(length of historical data, offset)	(2, 1)	(2, 1)	(2, 1)	(2, 1)
MM	(length of historical data, offset)	(2, 1)	(2, 1)	(2, 1)	(2, 1)
ARIMA	((no. of lag observations (p), degree of differencing (d), order of MA (q)), trend)	((1, 3, 2), 'c')	((3, 0, 3), 'c')	((0, 1, 3), 'c')	((2, 1, 0), 'c')
ETS	(trend, damped trend, seasonal)	('mul', False, None)	('add', True, None)	(None, False, None)	('add', True, None)
MLP	(inputs, nodes, epochs, batch size)	(1, 150, 100, 150)	(1, 150, 500, 100)	(10, 100, 100, 150)	(1, 150, 500, 100)
CNN	(inputs, filters, kernels, epochs, batch size)	(2, 256, 1, 100, 150)	(2, 256, 1, 500, 150)	(2, 256, 1, 500, 150)	(2, 256, 1, 500, 150)
LSTM	(inputs, nodes, epochs, batch size)	(1, 150, 100, 100)	(1, 150, 500, 150)	(1, 100, 500, 100)	(1, 150, 500, 150)
LSTM-I	(sequences, steps, filters, kernels, nodes, epochs, batch size)	(1, 2, 256, 1, 100, 100, 150)	(1, 2, 256, 1, 100, 100, 150)	(1, 2, 256, 1, 100, 500, 150)	(1, 2, 256, 1, 100, 100, 150)
LSTM-II	(sequences, steps, filters, kernels, nodes, epochs, batch size)	(2, 1, 256, 1, 100, 500, 150)	(2, 1, 256, 1, 100, 500, 150)	(2, 1, 256, 1, 150, 500, 100)	(2, 1, 256, 1, 100, 500, 150)

TABLE I: List of training hyperparameters chosen for each prediction model using the grid search framework [23].

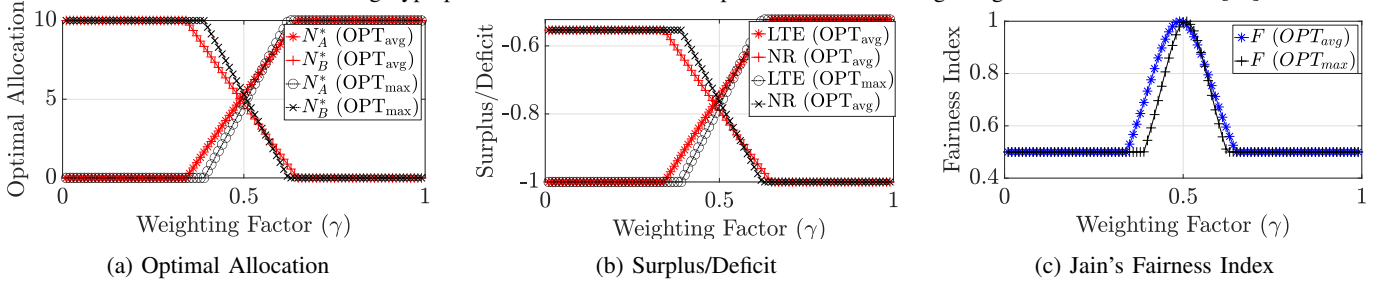


Fig. 5: Results for OPT_{max} versus OPT_{avg} for resource pool size $N_r = 10$ resources.

in deficits across all γ values, while OPT_{max} may result in surpluses, especially when one network has significantly higher priority (near γ values of 0 or 1), making OPT_{max} advantageous in such cases. Finally, for $N_r = 50$ resources, where the pool comfortably accommodates both mean and maximum demands, OPT_{max} outperforms OPT_{avg} for both networks, leading to surpluses. As the resource pool size approaches the maximum total demand, OPT_{avg} tends to allocate resources equal to the mean demand, resulting in deficits, whereas OPT_{max} results in over-provisioning.

In essence, our results underline the significance of γ in resource allocation decisions and demonstrate that the choice between OPT_{avg} and OPT_{max} depends on the resource pool size relative to network demands. OPT_{avg} excels in fairness but may cause deficits in limited resource scenarios. Conversely, OPT_{max} is preferable when resources are more abundant as it yields surpluses. These findings provide valuable insights to the controller, enabling it to fine-tune resource allocation strategies to suit diverse network conditions, thereby enhancing overall performance and user satisfaction.

V. CONCLUSIONS

In this work, we introduced ProSAS, an O-RAN-compatible solution for intelligent spectrum sharing between LTE and NR networks. ProSAS focuses on proactive, intent-driven spectrum management while minimizing resource surplus or deficit experienced by both networks. We demonstrated its effectiveness using real-world LTE resource usage data and synthetically generated NR data. Using these datasets, we developed an optimization scheme and outlined a deployment scenario aligning with O-RAN requirements. Our emphasis on real-world data and alignment with industry standards makes ProSAS both practical and pertinent for network operators.

REFERENCES

- [1] "Ericsson mobility report," June, 2023. [Online]. Available: <https://www.ericsson.com/en/reports-and-papers/mobility-report/reports>
- [2] S. Parkvall, E. Dahlman, A. Furuskar, and M. Frenne, "NR: The New 5G Radio Access Technology," *IEEE Communications Standards Magazine*, vol. 1, no. 4, pp. 24–30, 2017.
- [3] S. Gopal, D. Griffith, R. A. Rouil, and C. Liu, "5G NR-LTE co-existence: opportunities, challenges, and solutions," *arXiv preprint arXiv:2210.03906*, 2022.
- [4] N. Bui and J. Widmer, "OWL: A reliable online watcher for LTE control channel measurements," *Proceedings of the 5th Workshop on All Things Cellular: Operations, Applications and Challenges*, pp. 25–30, 2016.
- [5] J. Yoon, D. Jarrett, and M. Van der Schaar, "Time-series Generative Adversarial Networks," *Advances in Neural Information Processing Systems*, vol. 32, 2019.
- [6] S. Gopal, D. Griffith, R. Rouil, and C. Liu, "ProSAS: An O-RAN Approach to Spectrum Sharing between NR and LTE," <https://doi.org/10.18434/mds2-3178>, accessed: 2024-03-08.
- [7] S. Xu, J. Xin, S. Xiong, and Z. Sun, "Performance Analysis of CRS Interference Mitigation Algorithm in LTE and NR Coexistence Scenario," *2nd Information Communication Technologies Conference (ICTC)*, pp. 184–188, 2021.
- [8] L. Alexandre and S. A. Cerqueira, "Contribution for the Coexistence Analysis between 5G and 4G in the sub-1 GHz Band," *SBMO/IEEE MTT-S International Microwave and Optoelectronics Conference (IMOC)*, pp. 1–3, 2019.
- [9] L. Wan, Z. Guo, Y. Wu, W. Bi, J. Yuan, M. Elkashlan, and L. Hanzo, "4G/5G Spectrum Sharing: Efficient 5G Deployment to Serve enhanced Mobile Broadband and Internet of Things Applications," *IEEE Vehicular Technology Magazine*, vol. 13, no. 4, pp. 28–39, 2018.
- [10] T. Levanen, K. Ranta-Aho, J. Kaikkonen, S. Nielsen, K. Pajukoski, M. Renfors, and M. Valkama, "5G New Radio and LTE Uplink Coexistence," *IEEE Wireless Communications and Networking Conference (WCNC)*, pp. 1–6, 2018.
- [11] N. An, C. Wang, and W. Wang, "Interference Coexistence of 5G NR and LTE System Based on 2.1 GHz," *12th International Conference on Communication Software and Networks (ICCSN)*, pp. 90–94, 2020.
- [12] D. Li, D. Zhou, and L. Zhong, "Coexistence Analysis Between 5G NR and LTE Network at 1.8 GHz," *International Conference of Modern Trends in Information and Communication Technology Industry (MTICTI)*, pp. 1–6, 2021.
- [13] L. Wan, Z. Guo, and X. Chen, "Enabling Efficient 5G NR and 4G LTE Coexistence," *IEEE Wireless Communications*, vol. 26, no. 1, pp. 6–8, 2019.
- [14] R. Ratasuk, D. Zhou, and R. Sinha, "LTE-M Coexistence Within 5G New Radio Carrier," *IEEE 3rd 5G World Forum (5GWF)*, pp. 224–228, 2020.
- [15] M. Mozaffari, Y.-P. E. Wang, O. Liberg, and J. Bergman, "Flexible and Efficient Deployment of NB-IoT and LTE-MTC in Coexistence with

5G New Radio," *IEEE INFOCOM 2019-IEEE Conference on Computer Communications Workshops (INFOCOM WKSHPS)*, pp. 391–396, 2019.

- [16] M. H. C. Garcia, A. Molina-Galan, M. Boban, J. Gozalvez, B. Coll-Perales, T. Şahin, and A. Kousaridas, "A Tutorial on 5G NR V2X Communications," *IEEE Communications Surveys & Tutorials*, pp. 1–1, 2021.
- [17] O-RAN Alliance, "O-RAN Working Group 1 Use Cases Analysis Report," *O-RAN.WG1.Use-Cases-Analysis-Report-R003*, vol. 10.00, 2023.
- [18] R. Smith, C. Freeberg, T. Machacek, and V. Ramaswamy, "An O-RAN Approach to Spectrum Sharing Between Commercial 5G and Government Satellite Systems," *MILCOM 2021-2021 IEEE Military Communications Conference (MILCOM)*, pp. 739–744, 2021.
- [19] F. Mungari, "An RL Approach for Radio Resource Management in the O-RAN Architecture," *18th Annual IEEE International Conference on Sensing, Communication, and Networking (SECON)*, pp. 1–2, 2021.
- [20] L. Baldesi, F. Restuccia, and T. Melodia, "ChARM: NextG Spectrum Sharing Through Data-Driven Real-Time O-RAN Dynamic Control," *IEEE INFOCOM 2022-IEEE Conference on Computer Communications*, pp. 240–249, 2022.
- [21] Ł. Kułacz and A. Kliks, "Dynamic Spectrum Allocation Using Multi-Source Context Information in OpenRAN Networks," *Sensors*, vol. 22, no. 9, p. 3515, 2022.
- [22] A. Nielsen, *Practical Time Series Analysis: Prediction with Statistics and Machine Learning*. O'Reilly Media, 2019.
- [23] J. Brownlee, *Deep Learning for Time Series Forecasting: Predict the Future with MLPs, CNNs and LSTMs in Python*. Machine Learning Mastery, 2018.
- [24] O-RAN Alliance, "O-RAN Working Group 2 AI/ML Workflow Description and Requirements," *O-RAN.WG2.AI/ML*, vol. 1, 2021.

APPENDIX

A. Proof of Convexity for OPT_{max}

In this section, we show that OPT_{max} is a convex-optimization problem and hence has a global minimum. Mathematically, OPT_{max} is defined as:

$$\begin{aligned} OPT_{max} : \min_{N_A, N_B} & J_{max}(N_A, N_B | \gamma, M_{D_A}, M_{D_B}), \\ \text{s.t.} & N_A + N_B \leq N_R, \\ & 0 \leq N_A \leq N_R, \\ & 0 \leq N_B \leq N_R, \end{aligned} \quad (7)$$

where, M_{D_A} and M_{D_B} denote the maximum demand observed by the controller for each network and the objective function J_{max} is defined as:

$$J_{max} = \gamma \left(\frac{N_A - M_{D_A}}{M_{D_A}} \right)^2 + (1 - \gamma) \left(\frac{N_B - M_{D_B}}{M_{D_B}} \right)^2.$$

To show that (7) is a convex-optimization problem, we first compute the Hessian of its objective function and show that it is positive semidefinite. The Hessian of the objective function J_{max} is:

$$H = \begin{bmatrix} \frac{\partial^2 J_{max}}{\partial N_A^2} & \frac{\partial^2 J_{max}}{\partial N_A \partial N_B} \\ \frac{\partial^2 J_{max}}{\partial N_B \partial N_A} & \frac{\partial^2 J_{max}}{\partial N_B^2} \end{bmatrix} = \begin{bmatrix} \frac{2\gamma}{M_{D_A}^2} & 0 \\ 0 & \frac{2(1-\gamma)}{M_{D_B}^2} \end{bmatrix}.$$

For a Hessian of the bivariate function $F(x, y)$ to be positive semidefinite, as per Sylvester's criterion, the following two conditions must be satisfied:

- (a) $\frac{\partial^2 F}{\partial x^2} \geq 0$, and
- (b) $\frac{\partial^2 F}{\partial x^2} \frac{\partial^2 F}{\partial y^2} - \left(\frac{\partial^2 F}{\partial x \partial y} \right)^2 \geq 0$.

Since, both (a) and (b) are satisfied for the objective function J_{max} , its Hessian is positive semidefinite, and hence it is

convex. Also, the inequality constraints are convex, which makes the optimization problem, OPT_{max} , a convex optimization problem.

B. Proof of Convexity for OPT_{avg}

In this section, we show that OPT_{avg} is a convex-optimization problem and hence has a global minimum. Mathematically, OPT_{avg} is defined as:

$$\begin{aligned} OPT_{avg} : \min_{N_A, N_B} & J_{max}(N_A, N_B | \gamma, \mu_{D_A}, \sigma_{D_A}^2, \mu_{D_B}, \sigma_{D_B}^2), \\ \text{s.t.} & N_A + N_B \leq N_R, \\ & 0 \leq N_A \leq N_R, \\ & 0 \leq N_B \leq N_R, \end{aligned} \quad (8)$$

where, μ_{D_A} and μ_{D_B} correspond to the mean and $\sigma_{D_A}^2$ and $\sigma_{D_B}^2$ correspond to the variance of LTE and NR's demand, respectively, and the objective function J_{avg} is defined as:

$$J_{avg} = E \left[\gamma \left(\frac{N_A - D_A}{D_A} \right)^2 + (1 - \gamma) \left(\frac{N_B - D_B}{D_B} \right)^2 \right].$$

On solving the expectation we get:

$$\begin{aligned} J_{avg} &= E \left[\gamma \left(\frac{N_A^2}{D_A^2} + 1 - \frac{2N_A}{D_A} \right) + (1 - \gamma) \left(\frac{N_B^2}{D_B^2} + 1 - \frac{2N_B}{D_B} \right) \right], \\ &= 1 + \gamma N_A \left(N_A E \left[\frac{1}{D_A^2} \right] - 2E \left[\frac{1}{D_A} \right] \right) \\ &\quad + (1 - \gamma) N_B \left(N_B E \left[\frac{1}{D_B^2} \right] - 2E \left[\frac{1}{D_B} \right] \right). \end{aligned}$$

The second order Taylor series approximation of the expectation of $1/D_A$, $1/D_A^2$, $1/D_B$ and $1/D_B^2$ are as follows:

$$\begin{aligned} E \left[\frac{1}{D_A} \right] &= \frac{1}{\mu_{D_A}} + \frac{\sigma_{D_A}^2}{\mu_{D_A}^3}, & E \left[\frac{1}{D_A^2} \right] &= \frac{1}{\mu_{D_A}^2} + \frac{3\sigma_{D_A}^2}{\mu_{D_A}^4}, \\ E \left[\frac{1}{D_B} \right] &= \frac{1}{\mu_{D_B}} + \frac{\sigma_{D_B}^2}{\mu_{D_B}^3}, & E \left[\frac{1}{D_B^2} \right] &= \frac{1}{\mu_{D_B}^2} + \frac{3\sigma_{D_B}^2}{\mu_{D_B}^4}. \end{aligned}$$

On substituting the above expectation values in the objective function, we get:

$$\begin{aligned} J_{avg} &= 1 + \gamma N_A \left(N_A \left(\frac{1}{\mu_{D_A}^2} + \frac{3\sigma_{D_A}^2}{\mu_{D_A}^4} \right) - 2 \left(\frac{1}{\mu_{D_A}} + \frac{\sigma_{D_A}^2}{\mu_{D_A}^3} \right) \right) \\ &\quad + (1 - \gamma) N_B \left(N_B \left(\frac{1}{\mu_{D_B}^2} + \frac{3\sigma_{D_B}^2}{\mu_{D_B}^4} \right) - 2 \left(\frac{1}{\mu_{D_B}} + \frac{\sigma_{D_B}^2}{\mu_{D_B}^3} \right) \right). \end{aligned}$$

To show that (8) is a convex optimization problem and hence has a global minimum, we first compute the Hessian of the objective function and show that it is positive semidefinite. The Hessian of the objective function, J_{avg} is:

$$H = \begin{bmatrix} 2\gamma \left(\frac{1}{\mu_{D_A}^2} + \frac{3\sigma_{D_A}^2}{\mu_{D_A}^4} \right) & 0 \\ 0 & 2(1 - \gamma) \left(\frac{1}{\mu_{D_B}^2} + \frac{3\sigma_{D_B}^2}{\mu_{D_B}^4} \right) \end{bmatrix}.$$

Since both conditions of Sylvester's criterion are met for the objective function J_{avg} , its Hessian is positive semidefinite. Therefore, it is a convex function. Additionally, the inequality constraints are also convex, making the optimization problem, OPT_{avg} , a convex optimization problem.